Study on Strain-Rate Sensitivity of Cementitious Composites

Huang-Hsing Pan[1] and George J. Weng[2]

Abstract: In this study, we conduct a combined experimental and micromechanical investigation into the strain-rate sensitivity of concretes, with a special reference to the effect of aggregate concentration. We first measured the stress-strain relations of Type I portland cement with 0.45 water-to-cement ratio (w/c), and then those of the mortar containing sand aggregates of up to 50% volume concentration, over six orders of magnitude of strain rate, from 5×10^{-6}/s to 1×10^{-1}/s under compression. It was found that, at a given strain rate, the peak stress increases with the aggregate concentration but the peak strain tends to decrease with it. At a given aggregate concentration, the peak stress also increases with strain rate whereas the peak strain generally decreases with it. We then developed an inclusion-matrix type micromechanical model to simulate the behavior of the concrete. In this process the nonlinear viscoelastic behavior of the portland cement was modeled by a modified Burger's model with strain-rate dependent spring and dashpot elements, and the stress-strain relations of the mortar at various aggregate concentrations and strain rates were calculated from a two-phase composite model with a secant-moduli approach. It is shown that the measured data could be sufficiently well predicted by the developed micromechanics composite model.

DOI: 10.1061/(ASCE)EM.1943-7889.0000153

CE Database subject headings: Strain rates; Stress strain relations; Cement; Aggregates; Micromechanics; Composite materials.

Author keywords: Strain-rate sensitivity; Stress-strain behavior; Cement paste; Aggregates; Micromechanics; Cementitious composites; Peak stress and peak strain.

Introduction

Strain-rate sensitivity of concretes is a fundamental issue for their safe applications. For this reason the topic has received considerable attention in the past but, due to its complicated microstructures, concurrent studies involving both experimentation and micromechanical modeling are rare. Such correlated studies are particularly important in order to uncover the interplay between the aggregates and the cement paste, and this is the objective of the present study.

However, from the experimental side some observations have been made. For instance Harsh et al. (1990) have reported that the initial Young modulus and peak strength both increase with increasing strain rate, but the peak strain first decreases and then increases. The higher initial Young's modulus and peak strength have been attributed to the lower level of microcracking due to the higher rate loading (Yon et al. 1992). Brara et al. (2001) and Georgin and Reynouard (2003) have conducted some Hopkinson pressure bar tests to investigate the strain-rate sensitivity at high strain rate, and the tests have been supplemented with a discrete element simulation. The issue of damage has been examined by Sukontasukkul et al. (2004), and they found that the damage at peak load tends to increase with loading rate. Some projectile impact tests have been carried out to determine the impact resistance of high-strength concrete by Zhang et al. (2005), and they disclosed that, in order to increase the compressive strength, a reduction in the water-to-cement ratio and the reduction of the coarse aggregates were essential. Some dynamic tests on various types of concrete slabs and on concretes under confinement have also been conducted by Zineddin and Krauthammer (2007) and Forquin et al. (2008), respectively, and the results indicate that the dynamic strength are sensitive to the slab dimensions and the imposed strain rate.

From the theoretical side some numerical studies using ADINA have been conducted to study the strain-rate sensitivity of concrete (Bathe and Ramaswamy 1979; Tedesco et al. 1997). This issue has also been analyzed with a structure-dynamics approach (Chandra and Krauthammer 1995). Several other investigations have adopted a characterized technique with the peak load method to quantify the dynamic fracture properties of quasi-brittle materials (Tang et al. 1996; Lambert and Ross 2000). In addition Ragueneau and Gatuingt (2003) have developed some constitutive models to account for the strength-differential effect of concrete, and most recently, Zhu et al. (2009) have developed a wave propagation technique to examine the issue of stress uniformity along the thickness during the split Hopkinson pressure bar test. While investigations on the issue of strain-rate sensitivity are still ongoing, these experimental and theoretical studies have shed useful insights into the rate dependence of concrete behavior.

Most theoretical studies conducted thus far, however, did not take the advantage that concrete is essentially a composite material consisting of the cement paste and sand-stone aggregates. The properties of the concrete, such as the initial Young's modulus, the increase (or decrease) of its peak strength and peak strain, and the stress-strain relations under a constant strain-rate loading, are closely related to the properties of the cement paste and aggregates, and the volume concentration and aspect ratio of the latter. This observation has prompted us to undertake this

[1]Professor, Dept. of Civil Engineering, Kaohsiung Univ. of Applied Sciences, Kaohsiung 807, Taiwan. E-mail: pam@cc.kuas.edu.tw

[2]Professor, Dept. of Mechanical and Aerospace Engineering, Rutgers Univ., New Brunswick, NJ 08903 (corresponding author). E-mail: weng@jove.rutgers.edu

Note. This manuscript was submitted on March 4, 2009; approved on February 23, 2010; published online on February 25, 2010. Discussion period open until February 1, 2011; separate discussions must be submitted for individual papers. This paper is part of the ***Journal of Engineering Mechanics***, Vol. 136, No. 9, September 1, 2010. ©ASCE, ISSN 0733-9399/2010/9-1076–1082/$25.00.

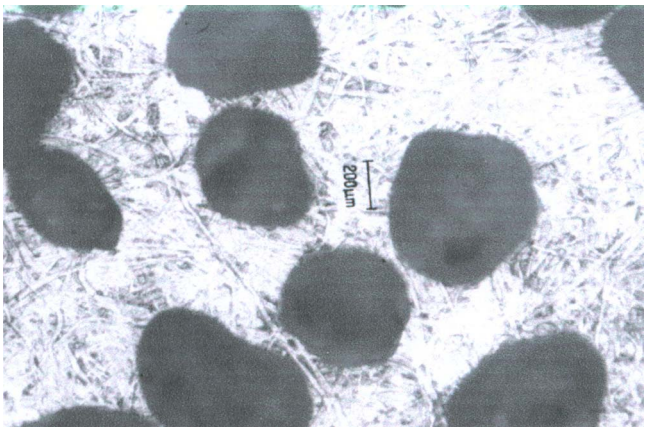

Fig. 1. Optical image of the aggregate morphology in the cementitious composite

micromechanics-based composite study. In order to verify the validity of the model and also to provide some new database, we have also conducted some new experiments on the strain-rate sensitivity of cement paste and mortar. This has been done over six orders of magnitude of strain rate, from 5×10^{-6}/s to 1×10^{-1}/s, and in the case of mortar, it covers three different aggregate concentrations at 30, 40, and 50%. Since the cement paste used in these tests was from the same sources, with the same water-to-cement ratio, these data could provide some benchmark value for others to compare.

In this composite model the matrix will be referred to as Phase 0 and the inclusions as Phase 1. The matrix phase, or binder here, is a broad combination of cement paste, fly ash, slag, silica fume, and other admixtures, and the inclusion phase represents the sand aggregates. The volume concentration of the rth phase will be denoted by c_r (i.e., $c_1+c_0=1$), and its bulk, shear, and Young's moduli by κ_r, μ_r, and E_r, respectively, and Poisson's ratio by ν_r.

Experiments for the Cement Paste and Mortar

The binder is Type I portland cement with a 0.45 water-to-cement ratio (w/c), and the aggregate is the sand consisting of 99% quartz. For the quartz sand the measured particle size was about 0.7–1.0 mm, with a specific gravity of 2.65, absorption of 0.24%, and a shape similar to a spheroid with an average aspect ratio (length-to-diameter ratio) of about $\alpha=1.13$. A typical optical image with a magnification of 50 times is given in Fig. 1. The experimental Young's modulus (initial slope) E_1 of the sand under various strain rates is given in Table 1 (it is rate-dependent). Its Poisson's ratio was determined to be $\nu_1=0.14$, calculated from the lateral strain measured at $\dot{\varepsilon}=1\times10^{-5}$/s. This value was assumed to remain constant, independent of the strain rate. Mortars were prepared using the same quality of cement paste with three different volume concentrations of quartz sand, at $c_1=0.3$, 0.4, and 0.5. The weights (in kilograms) of the constituent phases in a cubic meter of the cement-based materials are shown in Table 2, and, when divided by their respective density (cement of 3,150 kg/m^3 and water of 1,000 kg/m^3), it gives rise to the volume concentration of the individual phase. For instance under $c_1=0.3$, the volume concentration of cement is 912/3,150=0.29, and that of water is 410/1,000=0.41, and this gives the volume concentration of the matrix $c_0=0.29+0.41=0.7$, and thus the volume concentration of the sand aggregates is 0.3. It should also be noted that the w/c ratio has been maintained at a constant value in all cases, as 0.45=586/1,302=410/912, etc. All tests were conducted under compression.

Table 2. Weight of the Constituents in a Cubic Meter of Composite Materials (in Kilograms)

c_1	w/c	Cement	Water	Sand
0	0.45	1,302	586	—
0.3	0.45	912	410	795
0.4	0.45	782	352	1,060
0.5	0.45	652	293	1,325

Cylindrical test specimens were prepared using steel molds. For the strain rates less than the moderate strain rate (about 1×10^{-3}/s), 12 samples with six $50\phi\times100$ mm and six $100\phi\times200$ mm were made at each strain rate. When the applied strain rate was at moderate and higher values, i.e., 1×10^{-3}/s, 1×10^{-2}/s, or 1×10^{-1}/s, six samples with $50\phi\times100$ mm and three with $50\times50\times50$ mm were tested. At the lowest strain rate (5×10^{-6}/s), specimens fractured in approximately 60 min, and at the fastest rate (1×10^{-1}/s) specimens failed in about 0.2 s.

These specimens were tested under an material testing system (MTS) with an extensometer, at the material age of 28 days. Each sample was dried in the air 1 day before the test. The longitudinal and lateral strains were measured to plot the stress-strain curves of the cement paste and the mortar, and to determine their Young's modulus (the initial slope) and Poisson's ratio. These curves further served to determine the material constants of the cement paste and provided the data of the mortar for comparison with the developed theory.

These tests disclosed that, while the aggregate property was linear, those of the binder and mortar were nonlinear, with strong strain-rate sensitivity. Seven strain rates including 5×10^{-6}/s, 1×10^{-5}/s, 7.22×10^{-5}/s, 1×10^{-4}/s, 1×10^{-3}/s, 1×10^{-2}/s, and 1×10^{-1}/s were chosen to generate the stress-strain curves of the cement paste (binder) and the mortar separately, where the strain rate 7.22×10^{-5}/s was converted from ASTM C39 with a $150\phi\times300$ mm specimen at the loading velocity of 1.3 mm/min. The rate-dependent, nonlinear viscoelastic behavior of the binder will be modeled by a modified Burger's model as depicted in Fig. 2. The stress-strain curves for these tests are shown in Figs. 3–6, at four different aggregate concentrations.

We shall first use the result of Fig. 3 to construct a nonlinear Burger's model for the cement paste. After the composite model has been developed, we will come back to Figs. 4–6 so that the theory can be compared against the experiment.

Table 1. Young's Modulus of Quartz Sand at Different Strain Rates

	Strain rate $\dot{\varepsilon}$						
	5×10^{-6}/s	1×10^{-5}/s	7.22×10^{-5}/s	1×10^{-4}/s	1×10^{-3}/s	1×10^{-2}/s	1×10^{-1}/s
E_1 (GPa)	40.3	42.0	44.5	47.5	50.0	53.3	58.4

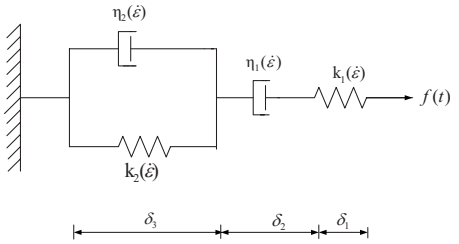

Fig. 2. Modified Burger's model with rate-dependent parameters for cement paste

Modified Burger's Model for the Cement Paste

The four-parameter Burger's model has been found to have a wide applicability in modeling the viscoelastic behavior of polymers (Wang and Weng 1992; Li and Weng 1994a,b). It has the virtue of an instantaneous response to represent the elastic strain, and a transient and steady creep that are common in the constant-stress creep test. In a recent study we have also found that it is sufficient to model the cement property at one given strain rate (Kuo et al. 2008). But when the tests span over six orders of magnitude in strain rate as is done in this study, we have found that the constant stiffness and viscosity assumption in each element could not capture the rate dependence of the cement paste over such a wide range of strain rate tested. We have discovered that when this four-parameter model was modified to allow the stiffness and viscosity parameters to be rate-dependent, the stress-strain relations of the cement paste could be captured. A modified Burger's model with such rate-dependent properties are shown in Fig. 1, where the rate-dependent spring and dashpot constants are denoted as $k_1(\dot{\varepsilon})$, $k_2(\dot{\varepsilon})$, $\eta_1(\dot{\varepsilon})$, and $\eta_2(\dot{\varepsilon})$, respectively. The model is effectively a nonlinear viscoelastic one.

Under a constant strain-rate loading, the governing differential equation for such a modified model can be established as

$$\ddot{f}(t) + \left(\frac{k_1}{\eta_1} + \frac{k_1}{\eta_2} + \frac{k_2}{\eta_2}\right)\dot{f}(t) + \frac{k_1 k_2}{\eta_1 \eta_2} f(t) = \frac{k_1 k_2}{\eta_2} w \qquad (1)$$

where $f(t)$=external load; t=loading time; and w=loading velocity given by the sum $\dot{\delta}_1+\dot{\delta}_2+\dot{\delta}_3$ (see Fig. 2). Then following the relation of $\dot{\varepsilon}=d\varepsilon/dt$=constant and by means of the interchange of independent variables related to t and ε, the applied load can be solved in terms of strain as

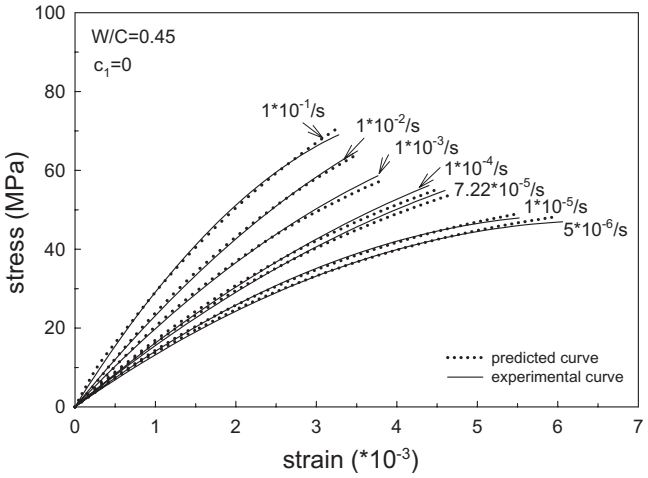

Fig. 3. Experiments and simulations for the cement paste with w/c =0.45

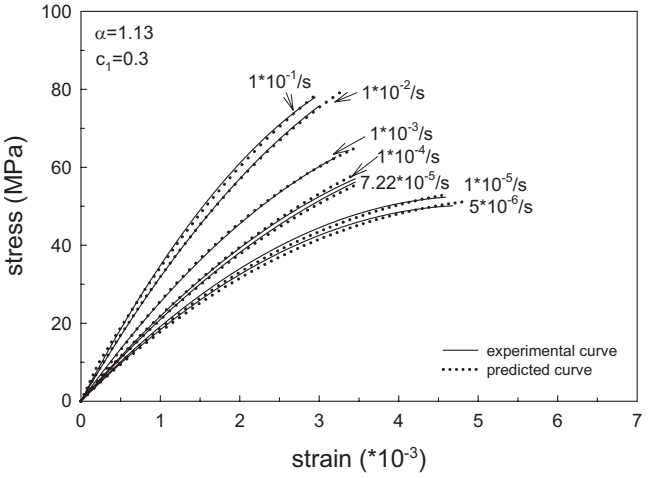

Fig. 4. Experiments and theoretical predictions for c_1=0.3 composite

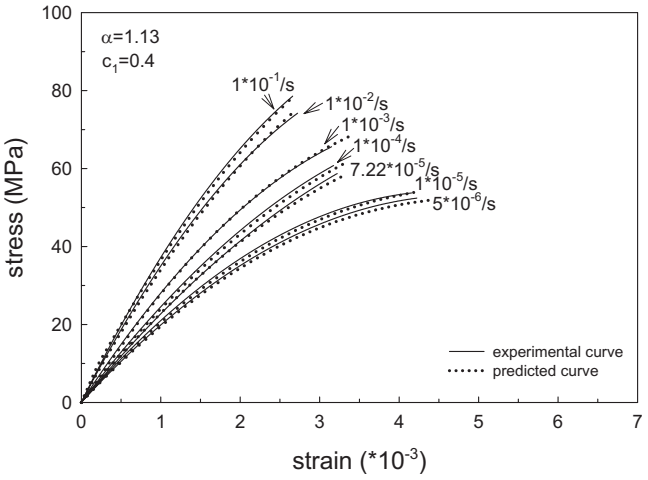

Fig. 5. Experiments and theoretical predictions for c_1=0.4 composite

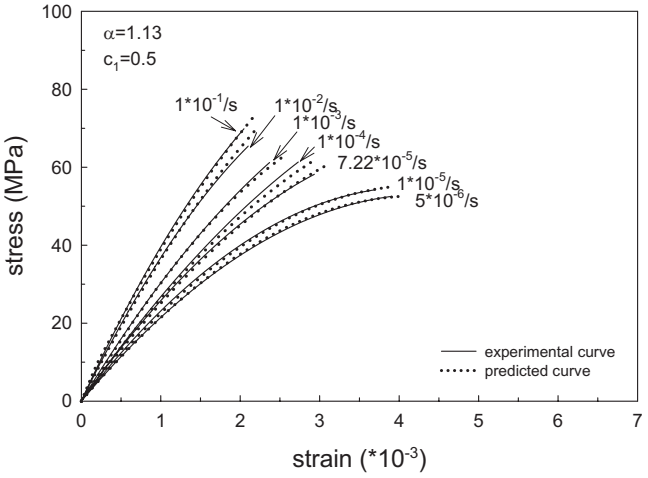

Fig. 6. Experiments and theoretical predictions for c_1=0.5 composite

$$f(\varepsilon) = b\left[e^{m_1(\varepsilon\times 10^3)} - \left(\frac{\eta_1 w + b}{b}\right) e^{m_2(\varepsilon\times 10^3)}\right] + \eta_1 w \tag{2}$$

where b=material parameter and m_1 and m_2=characteristic roots related to the four parameters of the rheological model, as

$$m_1 = \frac{\sqrt{[k_1\eta_2 + (k_1 - k_2)\eta_1]^2 + 4k_1k_2\eta_1^2} - k_1\eta_2 - (k_1 + k_2)\eta_1}{2\eta_1\eta_2} \tag{3}$$

$$m_2 = -\frac{\sqrt{[k_1\eta_2 + (k_1 - k_2)\eta_1]^2 + 4k_1k_2\eta_1^2} + k_1\eta_2 + (k_1 + k_2)\eta_1}{2\eta_1\eta_2} \tag{4}$$

The material constant b is related to the peak stress of the stress-strain curve of the cement paste. From an earlier test of the cement paste with w/c=0.45 under $\dot{\varepsilon}=1\times 10^{-5}$/s in Kuo et al. (2008), it was found that Eq. (2) carries the specific form

$$\frac{\sigma}{f_p} = 3.71[e^{m_1(\varepsilon\times 10^3)} - 1.009e^{m_2(\varepsilon\times 10^3)}] + 0.0356 \tag{5}$$

where σ and f_p=stress and peak stress of the cement binder, respectively, and the units of spring and dashpot constants are GN/m and GN-s/m, in turn. To correlate this relation with the tested specimen size and other applied strain rate $\dot{\varepsilon}$, this equation can be generalized to

$$\frac{\sigma}{f_p} = 3.71\left[e^{m_1(\varepsilon\times 10^3)} - \left(1 + 0.27\eta_1\frac{\dot{\varepsilon}}{A}\frac{L}{f_p}\right) e^{m_2(\varepsilon\times 10^3)}\right] + \eta_1\frac{\dot{\varepsilon}}{A}\frac{L}{f_p} \tag{6}$$

where A and L=area and length of the specimen, respectively. The stress-strain relation of the cement binder given in Eq. (6) can account for the effects of strain rate, peak stress, and the size of the specimen.

We have used this constitutive equation to simulate the tested stress-strain data of the cement paste at various specimen sizes and strain rates. The rate dependence of these four stiffness and viscosity parameters was calibrated to be

$$k_1(\dot{\varepsilon}) = 0.23(\log\dot{\varepsilon})^2 + 0.39\log\dot{\varepsilon} + 0.19$$

$$k_2(\dot{\varepsilon}) = -0.04(\log\dot{\varepsilon})^2 - 1.20\log\dot{\varepsilon} + 4.75$$

$$\eta_1(\dot{\varepsilon}) = 0.21(\log\dot{\varepsilon})^2 + 0.56\log\dot{\varepsilon} + 0.36$$

$$\eta_2(\dot{\varepsilon}) = -3.98(\log\dot{\varepsilon})^2 - 14.05\log\dot{\varepsilon} + 175.16 \tag{7}$$

With these constants and Eq. (6), the simulated and test results of the binder are shown in Fig. 3. Their close agreement suggests that together they can provide sufficiently accurate description for the constitutive behavior of the binder in the composite model.

Micromechanics-Based Composite Model for the Cementitious Composite

Since the cement and cement-based composites are under monotonically increasing load, the secant-moduli approach is particularly suitable for the calculation of the nonlinear stress-strain curves of the mortar. Such a procedure constitutes a continuous replacement of the elastic moduli by the corresponding secant moduli of the constituent phases so that the formulas for the effective elastic moduli of the composite can be used to determine the corresponding secant moduli of the composite. This concept has previously been adopted to study the plasticity of particle-reinforced metal-matrix composites without the rate sensitivity (Tandon and Weng 1988; Qiu and Weng 1992; Hu 1996) and the transient and steady state creep of metal-matrix composites (Pan and Weng 1993). A parallel approach based on the concept of secant-viscosity has also been introduced for the study of visco-plastic behavior of metal-matrix materials (Li and Weng 1997, 2007). These earlier studies all involve the metal matrix whose nonlinear state can be represented by von Mises' effective stress or strain, but such effective quantities do not exist for a nonlinear viscoelastic matrix. This is the problem we have here. To address this issue, we first recall that, by treating the sand aggregates as randomly oriented ellipsoidal (or spheroidal) inclusions, the effective bulk and shear moduli of the composite at a given c_1 can be written as (Pan and Weng 1995)

$$\frac{\kappa}{\kappa_0} = \frac{1}{1 + c_1(p_2/p_1)}; \quad \frac{\mu}{\mu_0} = \frac{1}{1 + c_1(q_2/q_1)} \tag{8}$$

based on the Eshelby (1957) and Mori-Tanaka (Mori and Tanaka 1973) approach, where parameters p_1, p_2, q_1, and q_2 depend on the moduli of the constituent phases, and volume concentration and shape of the inclusions through Eshelby's S tensor. The explicit forms of these parameters for ellipsoidal inclusions are listed in the Appendix, but with spheroidal inclusions a simpler version can be found in Tandon and Weng (1986). In particular when the inclusions can be idealized as spherical particles, one has (Weng 1984)

$$\frac{\kappa}{\kappa_0} = 1 + \frac{c_1(\kappa_1 - \kappa_0)}{c_0\alpha_0(\kappa_1 - \kappa_0) + \kappa_0}; \quad \frac{\mu}{\mu_0} = 1 + \frac{c_1(\mu_1 - \mu_0)}{c_0\beta_0(\mu_1 - \mu_0) + \mu_0} \tag{9}$$

where $\alpha_0=(1/3)(1+\nu_0)/(1-\nu_0)$ and $\beta_0=(2/15)(4-5\nu_0)/(1-\nu_0)$ This set of results is known to coincide with the lower bounds of Hashin and Shtrikman (1963) if the matrix is the softer phase, and with their upper bounds if it is the harder one.

The secant-moduli approach then replaces κ_0 and μ_0 of the matrix phase by its secant moduli κ_0^s and μ_0^s, at a given strain and strain rate, and this produces the effective secant moduli κ^s and μ^s, for the composite. The κ_0^s and μ_0^s themselves can be calculated from the secant Young's modulus E_0^s and Poisson's ratio through

$$\kappa_0^s(\varepsilon,\dot{\varepsilon}) = \frac{E_0^s(\varepsilon,\dot{\varepsilon})}{3(1-2\nu_0)}; \quad \mu_0^s(\varepsilon,\dot{\varepsilon}) = \frac{E_0^s(\varepsilon,\dot{\varepsilon})}{2(1+\nu_0)} \tag{10}$$

whereas E_0^s is evaluated from $E_0^s(\varepsilon,\dot{\varepsilon})=\sigma(\varepsilon,\dot{\varepsilon})/\varepsilon$, using the constitutive Eq. (6). After κ^s and μ^s have been obtained, the secant Young's modulus and secant Poisson's ratio of the composite can be determined from the isotropic connections

$$E^s(\varepsilon,\dot{\varepsilon}) = \frac{9\kappa^s(\varepsilon,\dot{\varepsilon})\mu^s(\varepsilon,\dot{\varepsilon})}{3\kappa^s(\varepsilon,\dot{\varepsilon}) + \mu^s(\varepsilon,\dot{\varepsilon})}; \quad \nu^s(\varepsilon,\dot{\varepsilon}) = \frac{3\kappa^s(\varepsilon,\dot{\varepsilon}) - 2\mu^s(\varepsilon,\dot{\varepsilon})}{6\kappa^s(\varepsilon,\dot{\varepsilon}) + 2\mu^s(\varepsilon,\dot{\varepsilon})} \tag{11}$$

The axial stress-strain curve of the cement-based composite then follows from

$$\bar{\sigma}_{11}(\varepsilon,\dot{\varepsilon}) = E^s(\varepsilon,\dot{\varepsilon})\bar{\varepsilon}_{11}(\varepsilon,\dot{\varepsilon}) \tag{12}$$

at a given strain rate $\dot{\varepsilon}$, where $\bar{\sigma}_{11}$ and $\bar{\varepsilon}_{11}$=stress and strain of the cement-based composite, respectively.

Table 3. Overall Peak Stress and Its Corresponding Strain of Cement-Based Materials

	$c_1=0$		$c_1=0.3$		$c_1=0.4$		$c_1=0.5$	
$\dot{\varepsilon}$	σ_p (MPa)	ε_p (10^{-3})	σ_p (MPa)	ε_p (10^{-3})	σ_p (MPa)	ε_p (10^{-3})	σ_p (MPa)	ε_p (10^{-3})
5×10^{-6}/s	46.95	6.06	50.11	4.68	52.40	4.22	52.53	3.91
1×10^{-5}/s	47.91	5.51	52.32	4.59	54.22	4.15	54.22	3.70
7.22×10^{-5}/s	54.89	4.60	56.19	3.45	58.71	3.22	58.18	2.93
1×10^{-4}/s	56.15	4.38	57.06	3.45	61.48	3.20	57.78	2.51
1×10^{-3}/s	58.61	3.77	65.59	3.21	65.57	3.14	61.22	2.37
1×10^{-2}/s	64.30	3.46	75.74	3.00	76.18	2.72	65.40	2.18
1×10^{-1}/s	69.03	2.28	77.99	2.95	78.56	2.66	71.89	2.10

Results and Discussions

Before we move on to the comparison between the theory and experiment, let us first examine the measured peak stress at which the stress reaches the maximum and then the decline, and the corresponding strain, the peak strain, of the cement paste and the mortar. These data are of some practical importance for design and application of mortar under compression. The results are given in Table 3, where the peak stress and peak strain are denoted by σ_p and ε_p, respectively. In general, the peak stress increases with increasing strain rate, and this is consistent with the report of Harsh et al. (1990). We also found that the overall peak strain tends to decrease with increasing strain rate, but for the mortar the decrease from 7.22×10^{-5}/s to 1×10^{-4}/s is not significant (at $c_1=0.3$ and 0.4 it remains almost constant). The overall trend spanning over the six orders of magnitude of the strain rate, however, suggests that the increase of the peak strength is usually accompanied by the reduction in peak strain. At a given strain rate, the peak strength tends to increase with increasing aggregate concentration, until c_1 reaches the high value of 0.5. At this high concentration it is possible that, after some prolonged compression, microcracks have developed and this in turn has led to the reduction of the compressive strength. The peak strain at each strain rate appears to be decreasing monotonically with the aggregate concentration over the entire range of strain rate.

The measured initial Poisson's ratio of cement paste ν_0 and the mortar ν are given in Table 4. At a given aggregate concentration this value does not change much with increasing strain rate, even though a slight reduction is observed. But at a given strain rate the measured Poisson's ratio decreases appreciably with c_1, for the Poisson's ratio of sand is noticeably lower than that of the cement paste. The measured peak stress and Poison's ratio listed in Tables 3 and 4 have some benchmark values for others to compare in the future. The Poisson's ratio of the cement paste ν_0 is also needed for the calculation of the secant bulk and shear moduli κ_0^s and μ_0^s of the cement paste in Eq. (10).

Table 4. Initial Poisson's Ratio of Cement-Based Materials

$\dot{\varepsilon}$	$c_1=0$	$c_1=0.3$	$c_1=0.4$	$c_1=0.5$
5×10^{-6}/s	0.183	0.174	0.171	0.169
1×10^{-5}/s	0.183	0.174	0.171	0.169
7.22×10^{-5}/s	0.182	0.173	0.171	0.167
1×10^{-4}/s	0.182	0.172	0.168	0.166
1×10^{-3}/s	0.182	0.172	0.168	0.166
1×10^{-2}/s	0.181	0.171	0.167	0.165
1×10^{-1}/s	0.180	0.170	0.166	0.164

Now let us compare the theory with the experiment by looking into the measured and the calculated stress-strain curves of the cement paste and mortar at three different volume concentrations of aggregates, $c_1=0$, 0.3, 0.4, and 0.5. These results are shown in Figs. 3–6, respectively. In each case the data have spanned over six orders of magnitude of strain rate, from 5×10^{-6}/s to 1×10^{-1}/s. We have made sure that the cement paste used in these tests was all with the same water-cement ratio, and all tested pieces were aged for the same 28 days to provide consistency. In the calculations the sand aggregates were taken to keep a constant Poisson's ratio at $\nu_1=0.14$, and the shape with an average aspect ratio at $\alpha=1.13$. The theoretical curves in Fig. 3 were carried out with the constitutive equation in Eq. (6) and the rate-dependent constants in Eq. (7). Reasonable simulation for the cement paste is observed. We then sued these cement properties in the secant-moduli approach outlined in Eqs. (8)–(12) to calculate the stress-strain curves of the cementitious composites at various concentrations of aggregates. The results are shown in Figs. 4–6. These results are strict predictions—not simulations—by the secant-moduli approach. No adjustable parameters are involved here. It is seen that the micromechanical composite model can capture the strain-rate sensitivity of the cementitious composites sufficiently well.

For the purpose of practical application of the proposed secant-moduli approach, it is worth noting that, since the aspect ratio of the aggregate is sufficiently close to 1, it might be useful to see how the predictions would turn out if it is simply taken as 1. In that case the simple formulas of Eq. (9) for spherical inclusions can be adopted as the starting point. We have found that in all cases considered here, this simple approximation does not jeopardize the accuracy of the predictions in any significant manner. For instance a typical result for $c_1=0.5$ at the strain rate of 5×10^{-6}/s is shown in Fig. 7, where the spherical-type approximation is seen to provide a sufficiently close agreement with the experimental curve. Also shown here is the extreme shape of a thin disk with $\alpha=0$, whose result is noticeably stiffer than the test data. We can conclude that, for all practical purposes, the simple formulas of spherical inclusions can be used to calculate the stress-strain curves of cementitious composites.

Conclusions

In this article we have carried out a combined experimental and micromechanical study on the strain-rate sensitivity of cement paste and cementitious composites under compression. This investigation covers six orders of magnitude of the strain rate from 10^{-6}–10^{-1}/s, involving aggregate concentrations from 0 (cement paste) to 0.5. Our test results indicate that the peak stress of the

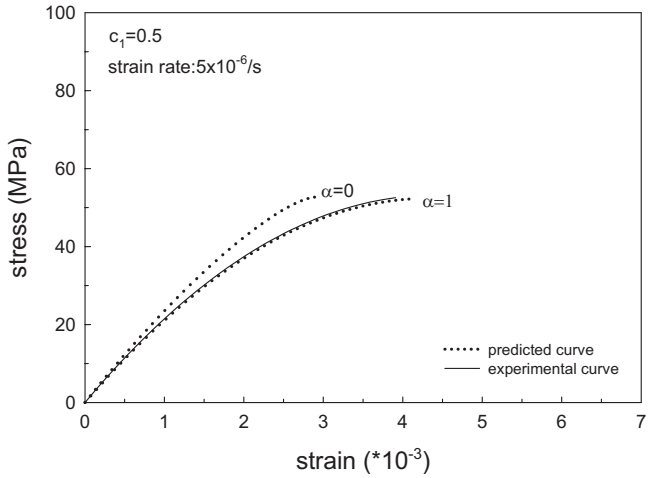

Fig. 7. Predictions using spherical inclusions ($\alpha=1$) and thin discs ($\alpha=0$) for the composite behavior under the strain rate $5\times10^{-6}/\mathrm{s}$

cement paste and mortar tends to increase with increasing applied strain rate and aggregate concentration. The peak strain, on the other hand, tends to decrease with both strain rate and aggregate concentration, but for the composite the decrease is not significant from $7.22\times10^{-5}/\mathrm{s}$ to $1\times10^{-4}/\mathrm{s}$. We have also found that the measured data for the cement paste can be modeled by a modified Burger's rheological model with strain-rate dependent spring and dashpot parameters. We have extended the concept of secant moduli in particle-reinforced metal-matrix composites to develop a micromechanics scheme for the nonlinear viscoelastic composites to calculate the stress-strain relations of the cementitious composites under a constant strain-rate loading. It is demonstrated that the calculated stress-strain relations at three different aggregate concentrations, over six orders of strain rate, are all in close agreement with the measured data.

Due to the consistency of the specimens prepared in the tests, and the systematic increase of strain rate and aggregate concentration adopted in the experiments, the measured data for the cement paste and mortar can serve as a benchmark for others to compare in the future. Moreover, the close agreement between the theoretical predictions and experimental data could result in the wide application of the developed micromechanical model in the future.

Acknowledgments

H. H. Pan was supported by the Taiwan National Science Council under Grant No. NSC 96-2221-E-151-046, and G. J. Weng was supported by the U.S. National Science Foundation, Division of Civil, Mechanical and Manufacturing Innovation, Mechanics and Structure of Materials Program, under Grant No. CMS-0510409.

Appendix. Components of p_1, p_2, q_1, and q_2 in Eq. (8) with Ellipsoidal Inclusions

Without any summation over any repeated indices and with i, j, and k always following the 1, 2, and 3 even permutation, we have (Pan and Weng 1995)

$$p_1 = 1 + c_1[b_1 + 2(b_2 + b_3 + b_4 + b_5)]/3$$

$$p_2 = (a_{11} + a_{12} + a_{13} + a_{21} + a_{22} + a_{23} + a_{31} + a_{32} + a_{33})/3$$

$$q_1 = 1 + c_1[2(b_1 - b_2 - b_3) + 7b_4 - 5b_5 + 6b_6]/15$$

$$q_2 = [3(b_{12} + b_{13} + b_{23}) + 2(a_{11} + a_{22} + a_{33}) - (a_{12} + a_{13} + a_{21} + a_{23} + a_{31} + a_{32})]/15$$

$$a_{ii} = [3(\kappa_1 - \kappa_0)(\mu_1 - \mu_0)^2(S_{jjjj}S_{kkkk} - S_{jjkk}S_{kkjj}) - (\mu_1 - \mu_0)(\kappa_1\mu_0 - \kappa_0\mu_1)(S_{jjjj} + S_{kkkk} - S_{jjkk} - S_{kkjj}) + 3\mu_0(\kappa_1 - \kappa_0)(\mu_1 - \mu_0) \times (S_{jjjj} + S_{kkkk}) + 3\kappa_0\mu_0(\mu_1 - \mu_0) + \mu_0(\kappa_1\mu_0 - \kappa_0\mu_1)]/A$$

$$a_{ij} = [3(\kappa_1 - \kappa_0)(\mu_1 - \mu_0)^2(S_{iikk}S_{kkjj} - S_{iijj}S_{kkkk}) - (\mu_1 - \mu_0)(\kappa_1\mu_0 - \kappa_0\mu_1)(S_{iikk} + S_{kkjj} - S_{iijj} - S_{kkkk}) - 3\mu_0(\kappa_1 - \kappa_0)(\mu_1 - \mu_0)S_{kkjj} + \mu_0(\kappa_1\mu_0 - \kappa_0\mu_1)]/A$$

$$b_{ij} = (1 - \mu_1/\mu_0)/[1 - 2S_{ijij}(1 - \mu_1/\mu_0)]$$

$$b_1 = a_{11}(S_{1111} - 1) + a_{21}S_{1122} + a_{31}S_{1133}$$

$$b_2 = [(a_{12} + a_{13})(S_{1111} - 1) + (a_{22} + a_{23})S_{1122} + (a_{32} + a_{33})S_{1133}]/2$$

$$b_3 = [a_{11}(S_{2211} + S_{3311}) + a_{21}(S_{2222} + S_{3322} - 1) + a_{31}(S_{3333} + S_{2233} - 1)]/2$$

$$b_4 = [(3a_{33} + a_{32})(S_{3333} - 1) + (3a_{23} + a_{22})S_{3322} + (3a_{13} + a_{12})S_{3311} + (3a_{32} + a_{33})S_{2233} + (3a_{22} + a_{23})(S_{2222} - 1) + (3a_{12} + a_{13})S_{2211} + 2b_{23}(2S_{2323} - 1)]/8$$

$$b_5 = [(a_{33} + 3a_{32})(S_{3333} - 1) + (a_{23} + 3a_{22})S_{3322} + (a_{13} + 3a_{12})S_{3311} + (a_{32} + 3a_{33})S_{2233} + (a_{22} + 3a_{23})(S_{2222} - 1) + (a_{12} + 3a_{13})S_{2211} - 2b_{23}(2S_{2323} - 1)]/8$$

$$b_6 = [b_{12}(2S_{1212} - 1) + b_{13}(2S_{1313} - 1)]/2$$

$$A = (\mu_1 - \mu_0)(\kappa_1\mu_0 - \kappa_0\mu_1)[S_{3333}(S_{1111} + S_{2222} - S_{1122} - S_{2211}) + S_{3322}(S_{1133} + S_{2211} - S_{1111} - S_{2233}) + S_{3311}(S_{1122} + S_{2233} - S_{1133} - S_{2222}) + S_{2211}(S_{1133} - S_{1122}) + S_{2222}(S_{1111} - S_{1133}) + S_{2233}(S_{1122} - S_{1111})] + 3(\kappa_1 - \kappa_0)(\mu_1 - \mu_0)^2[S_{3333}(S_{1122}S_{2211} - S_{1111}S_{2222}) + S_{3322}(S_{1111}S_{2233} - S_{1133}S_{2211}) + S_{3311}(S_{1133}S_{2222} - S_{1122}S_{2233})] + 3\mu_0(\kappa_1 - \kappa_0)(\mu_1 - \mu_0)(S_{1122}S_{2211} + S_{1133}S_{3311} + S_{2233}S_{3322} - S_{1111}S_{2222} - S_{2222}S_{3333} - S_{3333}S_{1111}) - \mu_0(\kappa_1\mu_0 - \kappa_0\mu_1)(S_{1111} + S_{1122} + S_{1133} + S_{2211} + S_{2222} + S_{2233} + S_{3311} + S_{3322} + S_{3333}) - 3\kappa_0\mu_0(\mu_1 - \mu_0)(S_{1111} + S_{2222} + S_{3333} - 1) - 3\kappa_0\mu_0\mu_1$$

To apply the secant-moduli approach, the elastic moduli of the matrix (Phase 0) need to be replaced by its corresponding secant moduli.

References

Bathe, K. J., and Ramaswamy, S. (1979). "On three-dimensional nonlinear analysis of concrete structures." *Nucl. Eng. Des.*, 52, 385–409.

Brara, A., Camborde, F., Klepaczko, J. R., and Mariotti, C. (2001). "Experimental and numerical study of concrete at high strain rate in tension." *Mech. Mater.*, 33, 33–45.

Chandra, D., and Krauthammer, T. (1995). "Strength enhancement in particulate solids under high loading rate." *Earthquake Eng. Struct. Dyn.*, 24, 1609–1622.

Eshelby, J. D. (1957). "The determination of the elastic field of an ellipsoidal inclusion, and related problems." *Proc. R. Soc. London, Ser. A*, 241, 376–396.

Forquin, P., Gary, G., and Gatuingt, F. (2008). "A testing technique for concrete under confinement at high rates of strain." *Int. J. Impact Eng.*, 35, 425–446.

Georgin, J. F., and Reynouard, J. M. (2003). "Modeling of structures subjected to impact: Concrete behaviour under high strain rate." *Cem. Concr. Compos.*, 25, 131–143.

Harsh, S., Shen, Z., and Darwin, D. (1990). "Strain-rate sensitive behavior of cement paste and mortar in compression." *ACI Mater. J.*, 87, 508–515.

Hashin, Z., and Shtrikman, S. (1963). "A variational approach to the theory of the elastic behaviour of multiphase materials." *J. Mech. Phys. Solids*, 11, 127–140.

Hu, G. (1996). "A method of plasticity for general aligned spheroidal void or fiber-reinforced composites." *Int. J. Plast.*, 12, 439–449.

Kuo, T. H., Pan, H. H., and Weng, G. J. (2008). "Micromechanics-based predictions on the overall stress-strain relations of cement-matrix composites." *J. Eng. Mech.*, 134, 1045–1052.

Lambert, D. E., and Ross, C. A. (2000). "Strain rate effects on dynamic fracture and strength." *Int. J. Impact Eng.*, 24, 985–998.

Li, J., and Weng, G. J. (1994a). "Strain-rate sensitivity, relaxation behavior and complex moduli of a class of isotropic viscoelastic composites." *J. Eng. Mater. Technol.*, 116, 495–504.

Li, J., and Weng, G. J. (1994b). "Effective creep behavior and complex moduli of fiber and ribbon-reinforced polymer-matrix composites." *Compos. Sci. Technol.*, 52, 615–629.

Li, J., and Weng, G. J. (1997). "A secant-viscosity approach to the time-dependent creep of an elastic-viscoplastic composite." *J. Mech. Phys. Solids*, 45, 1069–1083.

Li, J., and Weng, G. J. (2007). "A secant-viscosity composite model for the strain-rate sensitivity of nanocrystalline materials." *Int. J. Plast.*, 23, 2115–2133.

Mori, T., and Tanaka, K. (1973). "Average stress in matrix and average elastic energy of materials with misfitting inclusions." *Acta Metall.*, 21, 571–574.

Pan, H. H., and Weng, G. J. (1993). "Determination of transient and steady-state creep of metal-matrix composites by a secant moduli method." *Composites Eng.*, 3, 661–674.

Pan, H. H., and Weng, G. J. (1995). "Elastic moduli of heterogeneous solids with ellipsoidal inclusions and elliptic cracks." *Acta Mech.*, 110, 73–94.

Qiu, Y. P., and Weng, G. J. (1992). "A theory of plasticity for porous materials and particle-reinforced composite." *J. Appl. Mech.*, 59, 261–268.

Ragueneau, F., and Gatuingt, F. (2003). "Inelastic behavior modelling of concrete in low and high strain rate dynamics." *Comput. Struct.*, 81, 1287–1299.

Sukontasukkul, P., Nimityongskul, P., and Mindess, S. (2004). "Effect of loading rate on damage of concrete." *Cem. Concr. Res.*, 34, 2127–2134.

Tandon, G. P., and Weng, G. J. (1986). "Average stress in the matrix and effective moduli of randomly oriented composites." *Compos. Sci. Technol.*, 27, 111–132.

Tandon, G. P., and Weng, G. J. (1988). "A theory of particle-reinforced plasticity." *J. Appl. Mech.*, 55, 126–135.

Tang, T., Ouyang, C., and Shah, S. P. (1996). "A simple method for determining material fracture parameters from peak loads." *ACI Mater. J.*, 93, 147–157.

Tedesco, J. W., Powell, J. C., Ross, C. A., and Hughes, M. L. (1997). "A strain-rate-dependent concrete material model for ADINA." *Comput. Struct.*, 64, 1053–1067.

Wang, Y. M., and Weng, G. J. (1992). "The influence of inclusion shape on the overall viscoelastic behavior of composites." *J. Appl. Mech.*, 59, 510–518.

Weng, G. J. (1984). "Some elastic properties of reinforced solids, with special reference to isotropic ones containing spherical inclusions." *Int. J. Eng. Sci.*, 22, 845–856.

Yon, J.-H., Hawkins, N. M., and Kobayashi, A. S. (1992). "Strain-rate sensitivity of concrete mechanical properties." *ACI Mater. J.*, 89, 146–153.

Zhang, M. H., Shim, V. P. W., Lu, G., and Chew, C. W. (2005). "Resistance of high-strength concrete to projectile impact." *Int. J. Impact Eng.*, 31, 825–841.

Zhu, J., Hu, S., and Wang, L. (2009). "An analysis of stress uniformity for concrete-like specimens during SHPB tests." *Int. J. Impact Eng.*, 36, 61–72.

Zineddin, M., and Krauthammer, T. (2007). "Dynamic response and behavior of reinforced concrete slabs under impact loading." *Int. J. Impact Eng.*, 34, 1517–1534.